

Real-time Equation-of-Motion Coupled-Cluster Cumulant Green's Function Method: Heterogeneous Parallel Implementation Based on the Tensor Algebra for Many-body Methods Infrastructure

Himadri Pathak,^{*,†} Ajay Panyala,[†] Bo Peng,[‡] Nicholas P. Bauman,[‡] Erdal Mutlu,[†] John J. Rehr,[¶] Fernando D. Vila,^{*,¶} and Karol Kowalski^{*,‡}

[†]*Advanced Computing, Mathematics, and Data Division, Pacific Northwest National Laboratory, Richland, Washington 99354, USA*

[‡]*Physical Sciences Division, Pacific Northwest National Laboratory, Richland, Washington 99354, United States*

[¶]*Department of Physics, University of Washington, Seattle, Washington 98195, United States*

E-mail: himadri.pathak@pnnl.gov; fdv@uw.edu; karol.kowalski@pnnl.gov

Abstract

We report the implementation of the real-time equation-of-motion coupled-cluster (RT-EOM-CC) cumulant Green's function method [J. Chem. Phys. **152**, 174113 (2020)] within the Tensor Algebra for Many-body Methods (TAMM) infrastructure. TAMM is a massively parallel heterogeneous tensor library designed for utilizing forthcoming exascale computing resources. The two-body electron repulsion matrix elements are Cholesky-decomposed, and we imposed spin-explicit forms of the various operators when evaluating the tensor contractions. Unlike our previous real algebra Tensor Contraction Engine (TCE) implementation, the TAMM implementation supports fully complex algebra. The RT-EOM-CC singles (S) and doubles (D) time-dependent amplitudes are propagated using a first-order Adams–Moulton method. This new implementation shows excellent scalability tested up to 500 GPUs using the Zn-porphyrin molecule with 655 basis functions, with parallel efficiencies above 90% up to 400 GPUs. The TAMM RT-EOM-CCSD was used to study core photo-emission spectra in the

formaldehyde and ethyl trifluoroacetate (ESCA) molecules. Simulations of the latter involve as many as 71 occupied and 649 virtual orbitals. The relative quasiparticle ionization energies and overall spectral functions agree well with available experimental results.

Introduction

Photoemission spectroscopy (PES) is a widely used spectroscopic probe, covering a broad energy range from a few to several thousands of electronvolts (eV). The ubiquity of this technique is due, in part, to the variety of instruments available, ranging from small laboratory-based ones to synchrotron facilities.^{1,2} In the UV energy regime, PES provides access to the valence electronic structure, where low-energy electrons are the driving force of many chemical and biological processes.³ In the X-ray regime, core or X-ray photoelectron spectroscopy (XPS) is one of the most commonly used fingerprinting method in materials science, catalysis, and chemical engineering, where it is used to investigate the composition

and chemistry of materials at the atomic level.⁴⁻⁶ Given the importance of this experimental technique, complementary developments of accurate theoretical methods and associated software for the calculation and interpretation of XPS are crucial. Thus, a variety of methods have been developed in both the frequency and time domains. They are often used to predict the position of the main transition or quasiparticle (QP) peak. However, only advanced electron correlation methods can accurately simulate details of core-level photoemission spectra, particularly for the shake-up peaks, since these many-body phenomena reflect a complex interplay between electron correlation and orbital-reorganization effects. The time-independent coupled-cluster (CC) method and its many extensions⁷⁻¹⁶ have proven their utility in recovering electron correlation in a variety of problems for both ground and excited states. The ground-state CC method is size-extensive at any level of truncation of the excitation operators, and scales polynomially with the number of active orbitals. This makes these methods an attractive choice over other electron correlation methods, as they provide a balanced trade-off between the computation cost and desired accuracy. Furthermore, it is possible to improve the results systematically by incorporating more correlated determinantal spaces. The key feature of CC methods is the use of an exponential parameterization of the correlated ground state wavefunction $|\Psi\rangle$: $|\Psi\rangle = e^T |\Phi\rangle$, where T is the cluster operator, and $|\Phi\rangle$ is a reference wavefunction, which is usually but not necessarily a Hartree-Fock wavefunction. The cluster operator is defined by order of excitation, i.e. $T = T_1 + T_2 + \dots + T_n$ corresponding to singles, doubles, triples, ..., n -tuples, where $T_n = (\frac{1}{n!})^2 \sum_{a_1, \dots, a_n} t_{i_1 \dots i_n}^{a_1 \dots a_n} a_{a_1}^\dagger \dots a_{a_n}^\dagger a_{i_1} \dots a_{i_n}$. Here a_p^\dagger and a_p are creation and annihilation operators, respectively, associated with a set of $N_{so} = 2N_{bas}$ orthonormal spin-orbitals $\{\phi_p\}$, with N_{bas} being the number of basis functions. The indices i_n (a_n) correspond to orbitals that are occupied (unoccupied) with respect to the reference determinant.

When combined with the Green's function (GF) formalism in the frequency domain, the CC method provides an avenue to treat excited-state correlation effects that play a crucial role

in accurately simulating quasiparticles and satellite peaks in XPS.¹⁷⁻²⁶ However, for large systems, time-domain methods offer advantages over their frequency-domain counterparts by trading off memory resources for the serialization of the calculation. Therefore, there has been a lot of effort in developing efficient time-dependent approaches. Hoodbhoj and Negele,^{27,28} and Schönhammer and Gunnarsson²⁹ reported formulations of a time-dependent CC theory at about the same time. More recently, Kvaal proposed an orbital-adaptive time-dependent coupled-cluster method³⁰ relying on Arponen's bi-orthogonal formulation of CC theory,³¹ considering the complex analytic action formulation of the time-dependent variational principle (TDVP). Sato *et al.* have also developed a time-dependent optimized coupled-cluster method considering the real-action formulation of the TDVP,^{32,33} to approximately solve the time-dependent Schrödinger equation (TDSE) as a polynomial cost-scaling alternative to multi-configuration time-dependent Hartree-Fock methods.³⁴⁻³⁶ Both approaches^{30,32,33} choose to optimize the orbitals and ignore the one-body excitation (T_1) and de-excitation (Λ_1) operators. This approximation is well suited for strong-field physics, where consideration of optimal orbitals is crucial to obtain meaningful results. Such approaches provide a gauge-invariant description of the time-dependent properties of interest and satisfy the Ehrenfest theorem due to the use of variationally optimized orbitals.³⁷⁻⁴⁰ Despite this advantage, such methods^{30,32,33} are ill-suited for large-scale applications, especially when simulations involve core-hole states of chemical systems containing many active occupied electrons. Other developments in time-dependent electronic structure theory⁴¹ and time-dependent coupled-cluster methods^{39,42-60} are reviewed elsewhere.

Recently, we have developed a real-time equation-of-motion coupled-cluster (RT-EOM-CC) cumulant Green's function method⁶¹⁻⁶⁵ building on the Schönhammer and Gunnarsson formulation of the TDCC.²⁹ Subsequently several applications to the XPS of small molecules containing a few electrons in moderate size basis have been reported.⁶²⁻⁶⁵ In this methodology, as described in more detail below, the Green's function has a natural exponential cumulant form,

which is given by solutions to a set of coupled, first-order, nonlinear differential equations for the time-dependent CC amplitudes. While the traditional cumulant approximation is linear in the one-particle self-energy, the RT-EOM-CC approach builds in high-order nonlinear, nonperturbative contributions.

Even with their inherent memory usage advantage, large-scale time-dependent simulations are computationally challenging for chemically relevant systems that go beyond a handful of correlated electrons. However, thanks to recent advances in high-performance computing techniques that can take advantage of peta- and eventually exascale computational resources, such calculations are no longer insurmountable. In this article, we report the implementation of the RT-EOM-CC method with single and double excitations (RT-EOM-CCSD) within the Tensor Algebra for Many-body Methods (TAMM) infrastructure.^{66,67} TAMM is a massively parallel heterogeneous tensor library designed for developing quantum chemistry applications for forthcoming exascale supercomputers. Our RT-EOM-CC code uses Cholesky-decomposed two-electron repulsion matrix elements^{68,69} that aid in reducing the memory requirements and inter-node communication. Other speed-ups arise from spin-explicit evaluation of the coupled-cluster amplitudes. As discussed in the next section, the CC amplitudes in RT-EOM-CC are naturally complex valued. In contrast, our original implementation based on the real-valued Tensor Contraction Engine (TCE)^{62,64} used separate real-valued data structures to represent the real and imaginary parts and required two distinct subroutines to handle the propagation. Since the new TAMM implementation uses explicit complex algebra, only a single subroutine is required to handle the complex data, thus reducing the coding and data intricacy, even though complex algebra is more floating point operation intensive.

To demonstrate the capabilities of this new implementation, we study the core spectral functions of the formaldehyde and ethyl trifluoroacetate (ESCA) molecules and compare them with experimental spectra. We observe satisfying agreement between the computed and available experimental spectra. In addition to these systems, we

present parallel and storage performance for a few nominally “large” systems such as Zn-porphyrins, uracil, and the benzene-ammonia dimer.

Methods

Real-time Equation-of-Motion Coupled-Cluster Cumulant Green’s Function Method

The many-body Green’s function approach has proved very useful for the calculation of spectral functions of extended systems.^{70–73} By combining this approach with the CC method, we have developed a time-dependent CC cumulant Green’s function method⁶¹ that integrates the advantages of both. A detailed derivation of the complete method can be found elsewhere.^{62–65} In this section, we give a brief introduction to the RT-EOM-CC formulation. The goal is to construct the retarded core-hole Green’s function $G_c^R(\omega)$ and associated core spectral function $A_c(\omega) = (-1/\pi)\text{Im}G_c^R(\omega)$, by introducing a time-dependent coupled-cluster ansatz, $e^{iH\tau}|\Psi\rangle = |\Psi(\tau)\rangle = N_c(\tau)e^{T(\tau)}|\Phi\rangle$, which is a formal solution to the time-dependent Schrödinger equation $-i\frac{\partial}{\partial\tau}|\Psi(\tau)\rangle = H|\Psi(\tau)\rangle$. Here τ is time, and $|\Psi(\tau)\rangle$ is the fully correlated wavefunction for the $(N-1)$ -electron state, $H = \sum_{pq} h_{pq} a_p^\dagger a_q + \frac{1}{4} \sum_{pqrs} v_{pq}^{rs} a_p^\dagger a_q^\dagger a_s a_r$ is the nonrelativistic electronic Hamiltonian in second-quantization form, h_{pq} are the single-particle kinetic and electron-nuclei spinorbital integrals, and $v_{pq}^{rs} = \langle pq || rs \rangle$ are the usual antisymmetrized two-particle Coulomb integrals. $N_c(\tau)$ and $T(\tau)$ are, respectively, the time-dependent normalization constant and the time-dependent coupled-cluster operator. In principle, c can be any occupied orbital, but here we focus on deep core excitations. As usual, the p, q, r, s indices indicate generic spin-orbital states. In the current formulation, the time-independent reference determinant $|\Phi\rangle$ is a single $(N-1)$ -electron determinant formed from the N -electron Hartree–Fock states where the state c has been annihilated. Thus, it is important to note that T acts in the $(N-1)$ -electron space where c is now included in the set of unoccupied single-particle states. Following Ref. 61, the final form

of the equations of motion (EOMs) for $N_c(\tau)$, and $t_{ij\dots}^{ab\dots}(\tau)$ are:

$$-i\partial_\tau \ln N_c(\tau) = \langle \Phi | (H_N e^{T(\tau)})_C | \Phi \rangle + E_{N-1}^{\text{HF}} \quad (1)$$

$$-i\partial_\tau t_{ij\dots}^{ab\dots}(\tau) = \langle \Phi_{ij\dots}^{ab\dots} | (H_N e^{T(\tau)})_C | \Phi \rangle, \quad (2)$$

Here $H_N = \sum_{pq} f_{pq} \{a_p^\dagger a_q\}' + \frac{1}{4} \sum_{pqrs} v_{pq}^{rs} \{a_p^\dagger a_q^\dagger a_s a_r\}'$, and $\{\}'$ indicates that the normal ordering is done with respect to $|\Phi\rangle$ instead of the usual N -electron Hartree–Fock determinant. $E_{N-1}^{\text{HF}} = \langle \Phi | H | \Phi \rangle$ is the Hartree–Fock energy of the $(N-1)$ -electron systems. The Fock operator matrix elements are $f_{pq} = \varepsilon_p \delta_{pq} - v_{pc}^{qc}$, where c is the core-hole index as used above. The subscript "C" designates a connected part of a given operator expression.

Within this CC approximation, the retarded core-hole GF $G_c^R(\tau)$ is simply proportional to the normalization factor $N_c(\tau)$, since Eq. 1 has an exponential solution, and therefore $C_c^R(\tau)$, the retarded cumulant associated with c , is proportional to $\ln N_c(\tau)$:

$$G_c^R(\tau) = -i\Theta(\tau) e^{-i(\varepsilon_c + E_N^{\text{corr}})\tau} N_c(\tau) \quad (3)$$

$$= -i\Theta(\tau) e^{-i(\varepsilon_c + E_N^{\text{corr}})\tau} e^{C_c^R(\tau)} \quad (4)$$

$$C_c^R(\tau) = i \int_0^\tau \langle \Phi | (H_N e^{T(\tau')})_C | \Phi \rangle d\tau'. \quad (5)$$

Here ε_c is the single-particle Hartree–Fock energy of the core orbital c , and E_N^{corr} corresponds to the correlation energy of the N -electron closed-shell ground state. As a consequence, $G_c^R(\tau)$ can be expressed as the product of the free particle GF and the exponential of a cumulant, as expected within the cumulant approximation. We can now write down from Eq. 1 a complete expression for the time derivative of $C_c^R(\tau)$ within the single and double excitations approximation (CCSD):

$$-i\partial_\tau C_c^R = \langle \Phi | [H_N, T_2(\tau)] | \Phi \rangle + \frac{1}{2} \langle \Phi | [[H_N, T_1(\tau)], T_1(\tau)] | \Phi \rangle \quad (6)$$

Unlike conventional linear self-energy formulations, it is evident from Eq. 6 that the CCSD cumulant includes nonlinear, nonperturbative contributions.

The EOMs for the amplitudes within the CCSD

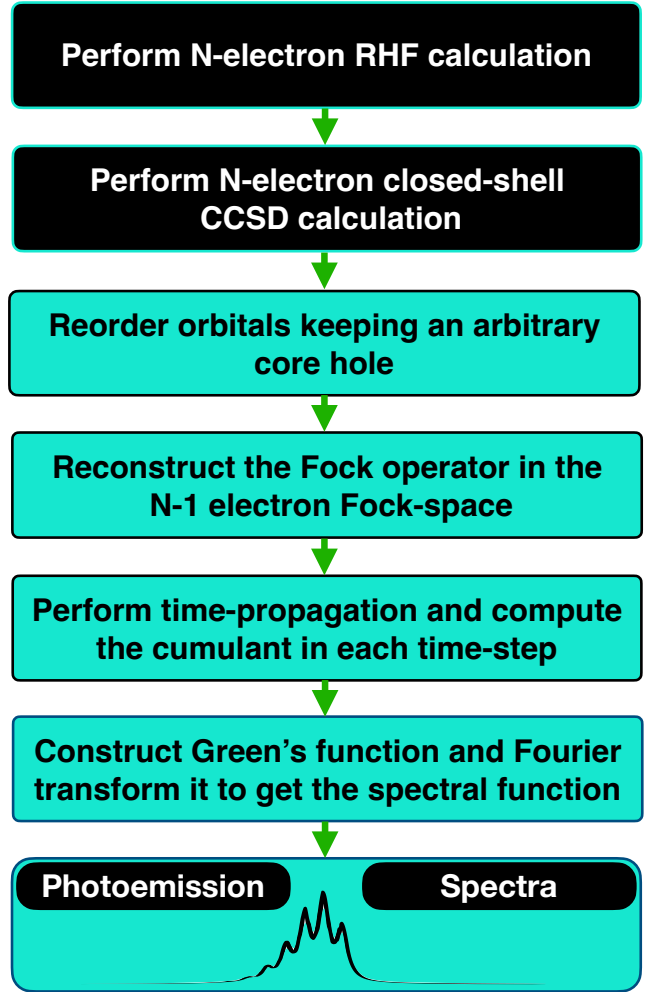


Figure 1: Real-time equation-of-motion coupled-cluster workflow.

approximation are obtained from Eq. 2 as

$$-i\partial_\tau t_i^a(\tau) = \langle \Phi_i^a | (H_N e^{T_1(\tau)+T_2(\tau)})_C | \Phi \rangle \quad (7)$$

$$-i\partial_\tau t_{ij}^{ab}(\tau) = \langle \Phi_{ij}^{ab} | (H_N e^{T_1(\tau)+T_2(\tau)})_C | \Phi \rangle, \quad (8)$$

where $t_i^a(\tau)$ and $t_{ij}^{ab}(\tau)$ are time-dependent singly and doubly excited cluster amplitudes.

Numerical Solution of the EOMs

To construct the core-hole spectral function $A_c(\omega)$ we need to compute the Green's function $G_c^R(\tau)$, which in turn depends on the cumulant $C_c^R(\tau)$ over the whole simulation range (Eqs. 5 and 6). Thus, the main task is to propagate Eqs. 7 and 8 in time, which provide solutions for both the T_1 and T_2 amplitudes needed to compute the cu-

mulant $C_c^R(\tau)$. Fig. 1 demonstrates a typical RT-EOM-CC workflow. Given that the RT-EOM-CC uses ground-state orbitals and the closed-shell CC ground-state energy, stationary restricted Hartree–Fock (RHF) and closed-shell coupled-cluster calculations are prerequisites to the time-dependent simulation. The computational cost of the RHF calculations is $\mathcal{O}(N_{bas}^3)$ while that for the CC part varies, depending on the imposed truncation in the excitation operator. The singles and doubles approximation used in this work scales as $\mathcal{O}(O^2V^4)$, where O and V denote the total number of occupied and virtual orbitals, respectively, and $O + V = N_{bas}$.

The first two ground-state calculation steps are common to most simulations involving core-hole excitations, but these are not the main bottlenecks since they need to be performed only once. After these, all calculations involving different core-hole states are unique and can run simultaneously. These calculations start by reading the N -electron closed-shell orbitals into the $(N - 1)$ -electron orbital space and then constructing the $(N - 1)$ -electron Fock matrix. At this point, the time-dependent simulation can start, where we propagate the CCSD amplitudes forward for the desired time, computing the time-derivative of the cumulant at each time step. It is worth pointing out that given that the time-dependent simulations involve an initial core hole, this is an open-shell problem and is roughly three times more expensive than its closed-shell counterpart in spin-explicit form.

As in our previous implementations, the first-order coupled nonlinear simultaneous differential equations for the amplitudes are integrated using the first-order Adams–Moulton method,⁷⁴ also known as the implicit trapezoidal rule. In this approximation the $t_{ij\dots}^{ab\dots}(\tau)$ are propagated with:

$$\begin{aligned}
 t_{ij\dots}^{ab\dots}(\tau + \Delta\tau) &= t_{ij\dots}^{ab\dots}(\tau) \\
 &+ \frac{i}{2}\Delta\tau \left(\left\langle \Phi_{ij\dots}^{ab\dots} \left| (H_{Ne}^{T(\tau)})_C \right| \Phi \right\rangle \right. \\
 &+ \left. \left\langle \Phi_{ij\dots}^{ab\dots} \left| (H_{Ne}^{T(\tau+\Delta\tau)})_C \right| \Phi \right\rangle \right), \quad (9)
 \end{aligned}$$

where $\Delta\tau$ is the simulation time-step. The propagation starts with the initial conditions $T_1 = 0$ and $T_2 = 0$. Since the Adams–Moulton method is im-

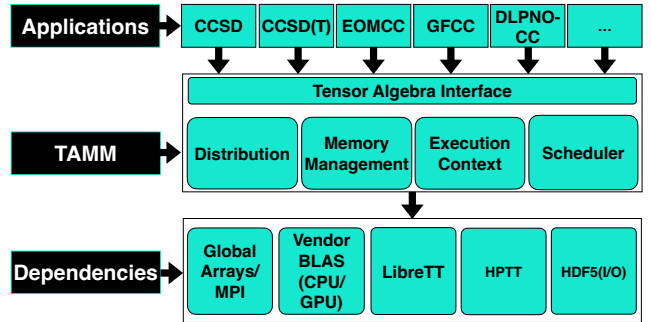


Figure 2: Overview of the Tensor Algebra for Many-body Methods (TAMM) framework.

PLICIT, the values of the amplitudes at $(\tau + \Delta\tau)$ depend on themselves. Thus, to solve Eq. 9 we use a fixed-point iteration scheme at each time step. Other methods of solution that use a variable time step and are more stable than fixed-point iteration are currently under development. After completion of the time propagation, the remainder of the workflow is not compute-intensive, since it only involves forming the time-dependent Green’s function from the cumulant, and then Fourier-transforming to obtain the spectral function in the frequency domain.

RT-EOM-CC Implementation in Tensor Algebra for Many-body Methods Infrastructure

The Tensor Algebra for Many-body Methods (TAMM) library^{66,80} is a massively parallel, heterogeneous tensor algebra library. It provides a computational infrastructure (see Fig. 2) that can achieve scalable performance. Furthermore, it allows portable implementations of many-body methods both on existing and forthcoming exascale super-computing platforms.

High-dimensional tensor contractions are the most compute-intensive components of the RT-EOM-CC method. Within the single and double excitations approximation (RT-EOM-CCSD), the most expensive tensor contraction is of the form $R(V, V, O, O) = \alpha \times v(V, V, V, V) \times t_2(V, V, O, O)$, involving four-dimensional tensors, the antisymmetrized two-body matrix elements v , and the two-body CC excitation operator t_2 , α is a scalar pre-factor. These multi-dimensional tensor con-

Table 1: Structural features of TAMM, including various used third-party dependency libraries.

Third-party dependencies	Global Arrays, ⁷⁵ BLIS, ⁷⁶ vendor BLAS/LAPACK, cuBLAS/rocBLAS/oneMKL HPTT, ⁷⁷ TALSH, ⁷⁸ LibInt2 ⁷⁹
Programming Languages	C++17, CUDA, HIP, SYCL, MPI, OpenMP
Precision	Double
Data Types	Real, Complex
Supports Restart Capabilities?	Yes
I/O requirements	Minor

tractions are not only computational- but also communication-intensive. There have been many efforts to develop specialized parallel tensor algebra libraries, including automated code generators and better memory management to facilitate these demanding tensor contractions.^{81–84} The TAMM library is one such effort aiming to achieve scalable performance on several heterogeneous architectures, by delivering a common platform for the portable implementation of numerous many-body methods. TAMM provides a variety of features to users including the ability to specify and manipulate tensor distribution, memory management, and scheduling of tensor operations. In addition, it supports both complex and mixed real-complex algebra for mathematical operations.

A summary of structural features and third-party libraries for the TAMM library is shown in Table 1. TAMM uses Global Arrays⁷⁵ and Message Passing Interface (MPI) to achieve scalable parallelization on distributed memory platforms, while using optimized libraries that help efficient intra-node execution of the tensor operation, both in CPU kernels and accelerators. TAMM also uses multi-granular dependence analysis and task-based execution to execute operations. First, it constructs a macro operation graph by analyzing the dependencies between various operations. When two operations share the same data structure, with one of them writing to the other, they are in conflict and impossible to execute in parallel. The operation graph is analyzed to identify and order the non-parallel operations to minimize the required numbers of synchronizations. The possible scheduled operations are executed in a single program multiple data fashion. Such executions are compatible with MPI, and their collective executions are per-

formed on a given MPI communicator. Various tasks constitute an operation, which is produced using task iterators. Each task performs part of the computation, usually adding a block of data to the output tensor. A given task is migratable and can be scheduled for execution on any compute node or processor core until its execution begins. The data needed for a job are transported to its location once the execution of the process has started. At this stage, migration of tasks is no longer possible and they are bound to process. TAMM’s GPU execution scheme uses localized summation loops to minimize the transfer of output blocks from GPUs to CPUs. This helps to reduce the data transmission between CPUs and GPUs by keeping the output block that is being updated by several input tensor blocks on the GPU until all updates are complete.

Programming Models, Software Dependencies, I/O, Restart/Checkpoint Capabilities

Memory demands, operation count, and time-to-solution are three main concerns that limit large-scale CC calculations. This is further complicated when extending the CC formalism to the time domain. To combat these hindrances, various techniques and features were incorporated during the implementation of the RT-EOM-CCSD method.

In canonical spin-orbital CC calculations, the four-dimensional electron repulsion integral (ERI) tensors are easily the largest memory-demanding objects. The storage requirement for the ERI tensor in its full spin-orbital form is of order N_{so}^4 , and they must undergo a tensor transformation from the atomic-orbital to molecular-orbital basis which scales as $\mathcal{O}(N_{bas}^5)$. In our RT-EOM-CC implementation, we employed Cholesky decomposition^{85–89}

of the ERI tensors to ease the memory/storage demands and increase the data locality resulting in reduced communication. We leveraged the same Cholesky decomposition previously implemented using the TAMM library,^{68,69} which is an on-the-fly pivoting decomposition of the two-body ERIs. The resulting Cholesky bases are three-index quantities that reduce the storage requirements from order N_{so}^4 to KN_{so}^2 , where $K \sim \mathcal{O}(N_{bas})$ is the number of Cholesky bases. In addition, the atomic-orbital to molecular-orbital transformation is conducted on the Cholesky bases rather than directly on the ERI, thus reducing the scaling of the transformation from $\mathcal{O}(N_{bas}^5)$ to $\mathcal{O}(N_{bas}^4)$. The accuracy of the correlation calculations employing the Cholesky bases in comparison with the canonical results is well-controlled through adjusting the diagonal cutoff in the Cholesky decomposition.

The next largest memory-demanding objects, after the ERIs, are the T_2 amplitudes. In a naive spin-orbital implementation, the memory requirement for all elements of the T_2 operator is $16O^2V^2$. The declaration includes 16 possible combinations of spins for the four indices, most of which do not contribute or are over-specified as they are equivalent through permutational symmetry. In our RT-EOMCC methodology, we implemented the spin-integrated form of equations. Only unique spin combinations of tensors with a non-zero contribution, including intermediates, are programmed. For the T_2 amplitudes, this means only three spin cases are necessary ($t_{\alpha\alpha}^{\alpha\alpha}$, $t_{\beta\beta}^{\beta\beta}$, and $t_{\alpha\beta}^{\alpha\beta}$), reducing the memory requirements to $\sim \frac{3}{16}$ that of the full T_2 operator. Memory requirements are reduced for other operators as well. Since non-contributing spin combinations are removed, and only unique spin cases are specified, the overall operation count is significantly reduced. The memory requirements of various systems with various large systems with 760 to 2450 spin-orbital functions can be seen in Table 2. In this Table, the memory requirement for the cluster amplitudes reflects the sum of the three timeline tensors needs for the iterative update given by Eq. 9. The combination of Cholesky-decomposed ERIs and spin-integrated equations allows for simulations with hundreds of orbitals on moderately sized computer clusters.

Another challenging aspect of RT-EOM-CC calculations is that it is necessary to propagate for a sufficiently long time to have well-resolved spectra. In practice, shared computing resource usually do not allow simulations to propagate for enough time in a single run to achieve sufficient resolution. Furthermore, it is important to be able to track simulations and adjust/optimize the time propagation parameters promptly, before a long time has elapsed. For these reasons, checkpointing and restart capabilities were imperative in our RT-EOM-CCSD implementation. Restarting the time-propagation algorithm at any i^{th} step requires the T amplitudes of the $(i-1)^{\text{th}}$ and i^{th} time steps, in addition to the Fock and Cholesky-decomposed ERIs. Parallel read and write capabilities in the TAMM library allow for periodic checkpointing while minimizing their impact on the overall computational time.

Geometries, Basis Sets, and Computational Details

In this study, we perform RT-EOM-CC simulations of two molecules, formaldehyde and ethyl trifluoroacetate (ESCA), in order to compare to previous theoretical and experimental results. For formaldehyde, we used the experimental geometry⁹⁰ and studied both C and O core ionizations using either the aug-cc-pVDZ,⁹¹ aug-cc-pVTZ,⁹¹ or Sapporo-TZP^{92,93} basis sets for all atoms in the molecule. Given that the ESCA molecule contains four C atoms, we computed ionization spectra from each of them. These calculations were performed with the Sapporo-TZP basis set for all the first-row elements, while for the H atom we used the aug-cc-pVDZ basis set. Since a complete experimental geometry of the ESCA molecule is not available, we used the one obtained from a B3LYP/aug-cc-pVTZ optimization.⁹⁴ The real-time time-propagation used a time-step of 0.015 au (~ 0.36 as) for formaldehyde and 0.01 au (~ 0.24 as) for the ESCA molecule, with a convergence cutoff of 10^{-4} for the fixed-point micro-iteration solution of the implicit first-order Adams–Moulton integrator. The total propagation time was 450 au (~ 11 fs) for formaldehyde and 100 au (~ 2.5 fs) for ESCA. All stationary calculations were performed with a linear

Table 2: Workflow memory requirements for the TAMM implementation of RT-EOM-CCSD for systems with Sapporo-TZP basis set for all atoms except H, for which we use aug-cc-pVTZ, using a Cholesky vectors diagonal cutoff of 10^{-6} , and linear dependence threshold of 10^{-6} .

System	Configuration Space					T_2 amplitude (GB)	Cholesky vectors (GB)	# of Cholesky vectors
	N_{so}	n_{occ}^α	n_{occ}^β	n_{vir}^α	n_{vir}^β			
Uracil	760	29	28	351	352	3×4.5	26.2	2044
ESCA	880	36	35	404	405	3×9.2	40.6	2423
Benzene-Ammonia	940	26	25	444	445	3×5.8	49.5	2457
Zn-porphyrin	2450	95	94	1130	1131	3×510.2	876.6	6258

dependence threshold for the basis sets of 10^{-6} , SCF convergence cutoff of 10^{-8} au for the energy, Cholesky diagonal cutoff of 10^{-6} and a CCSD convergence cutoff of 10^{-8} au. None of the virtual orbitals are frozen in any of our simulations.

Results and Discussion

Performance Analysis

As described in previous sections, a simulation is divided into a series of “macro-iterations” associated with each time step, and within each macro-iteration, many “micro-iterations” are performed to solve Eq. 9. Thus, the fundamental parallel performance metric for RT-EOM-CC is the “*time per micro-iteration*” associated with the calculation of the matrix elements in Eq. 9. In order to investigate the performance and scalability of the new optimized TAMM implementation of RT-EOM-CCSD, we have performed a series of calculations on the “pre-production” NERSC Perlmutter system (Nvidia A100). If the scaling is ideal, the total compute time is inversely proportional to the total number of allocated processors provided the total number of mathematical operations in each test case remains the same. Figure 3 shows the scalability of the TAMM implementation of RT-EOM-CCSD for Zn-porphyrin using the aug-cc-pVDZ basis set, which results in a total of 655 basis functions ($n_{occ}=94$, $n_{vir}=561$) after pruning 122 linear dependencies. Our time-dependent simulations involve a configuration space of $n_{occ}^\alpha = 95$, $n_{vir}^\alpha = 560$, $n_{occ}^\beta = 94$, $n_{vir}^\beta = 561$. We explore scaling between 200 and 500 GPUs (50 to 125 nodes given that each node is connected to 4 GPUs), using the per-

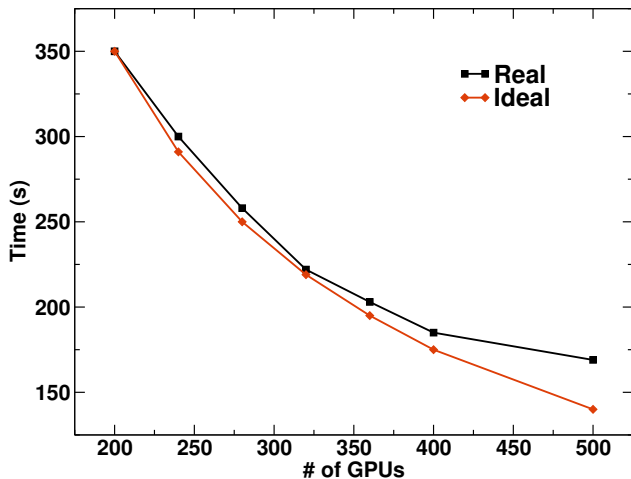


Figure 3: Real vs ideal single micro-iteration time as a function of number of GPUs for Zn-porphyrin using 655 basis functions.

formance with 200 GPUs as the reference. Figure 3 also shows the ideal theoretical scaling. In this range, we observe a nearly ideal drop in the computation time for each micro-iteration, very close to the theoretical limit. The parallel efficiency remains high (i.e. higher than 94%) up to 400 GPUs, after which it drops to 83% for 500 GPUs.

Spectral Function Results

The high quality of the RT-EOM-CC results has been previously demonstrated.^{63,65} Thus here we focus on showcasing the new capabilities of the RT-EOM-CCSD TAMM implementation for more complex systems. For this purpose, we have simulated formaldehyde (H_2CO) and ethyl trifluoroacetate (ESCA). For formaldehyde, we focus on the satellite region of the C and O core spectral func-

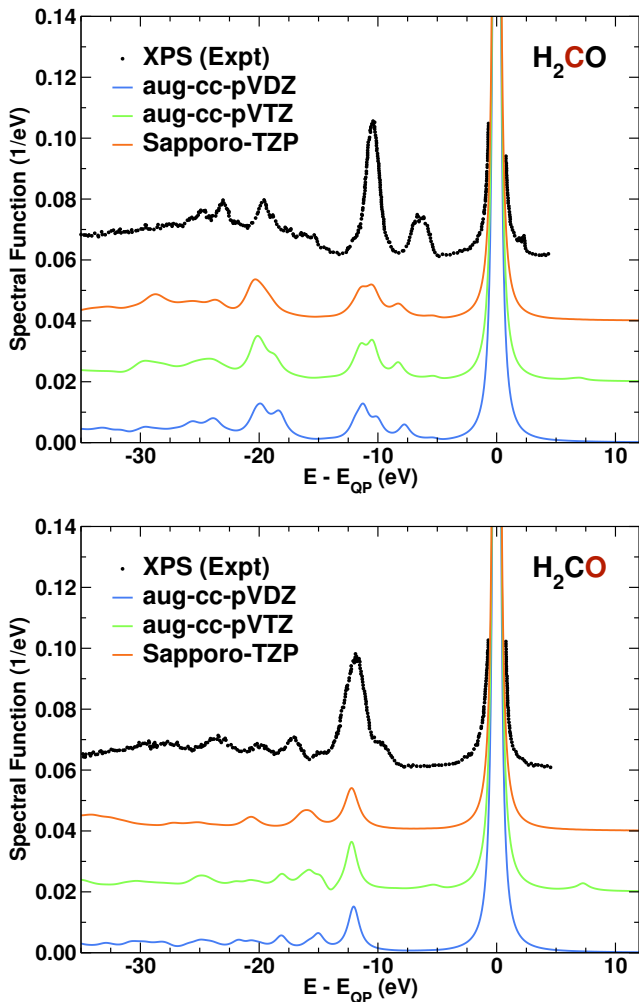


Figure 4: Comparison of satellite regions of the C (top) and O (bottom) RT-EOM-CCSD core spectral functions to the XPS experiment⁹⁵ for formaldehyde (H_2CO) as a function of basis set. The data has been shifted so that the quasiparticle peak is at 0 eV.

tions (Fig. 4). We find that the theory reproduces the XPS semi-quantitatively, with the position of most of the satellite features relative to the quasiparticle peak in reasonable agreement with experiment. The relative intensities of the peaks are not as well reproduced, probably due to i) the limitations of the local valence basis set used that misses the continuum background contribution, and ii) the limitations of the RT-EOM-CCSD to include all the relevant excitations in this energy range.

For the case of the ESCA molecule, shown in Fig. 5, we calculated the C core spectral function for each of the inequivalent C atoms in the system. The agreement with experiment is excellent,

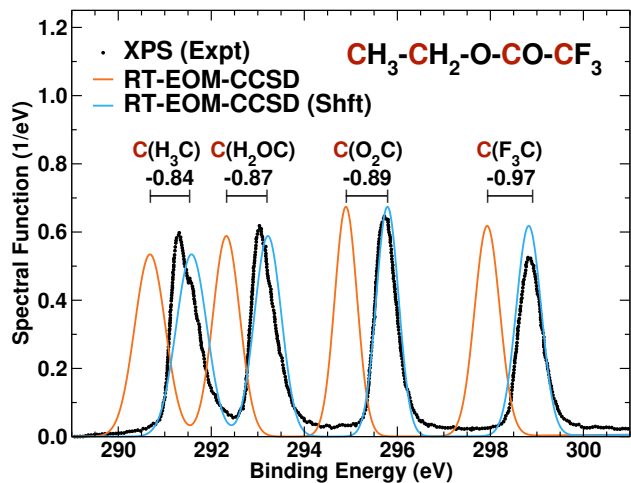


Figure 5: Comparison of the RT-EOM-CCSD/Sapporo-TZP C core spectral functions (red) to the experimental⁹⁴ XPS (black dots) for the ethyl trifluoroacetate (ESCA) molecule. Each peak corresponds to an individual C core ionization and has been broadened to match the vibrational experimental broadening. Also shown are the same results shifted by 0.89 eV (blue).

apart from a nearly-constant overall underestimation of the binding energies. When the underestimation shift is removed, the relative mean absolute error is only 0.04 eV. We also find that, unlike for the satellite peaks in H_2CO , the relative intensities of the ESCA quasiparticle peaks are qualitatively reproduced by the theory. By fitting the experiment to a skew Gaussian distribution (to account for the vibrational asymmetry), we find that the intensities of the $\text{C}(\text{H}_2\text{OC})$, $\text{C}(\text{O}_2\text{C})$ and $\text{C}(\text{F}_3\text{C})$ peaks relative to the $\text{C}(\text{H}_3\text{C})$ one are 0.81, 0.90 and 0.91, respectively, while for the theory the ratios are 0.94, 0.91 and 0.96. It was speculated⁹⁴ that some of the intensity of the different C quasiparticle peaks might originate from underlying satellite peaks from lower energy cores. We find that for each of the individual spectral functions the first satellite peaks appear more than 10 eV above the quasiparticle, and thus all the intensity observed for the peaks between 291 and 299 eV can be assigned exclusively to the quasiparticle transitions.

Conclusions

We have successfully implemented the RT-EOM-CCSD method within the parallel TAMM infrastructure using Cholesky decomposed two-body repulsion matrix elements. This implementation eliminates the memory bottleneck of the original approach associated with storing two-electron integrals. Unlike our earlier TCE-based RT-EOM-CCSD implementation, which relied only on real algebra, our new TAMM implementation supports explicit complex algebra. This implementation is also flexible regarding the choice of the reference function (i.e. where the hole state is located), and has checkpointing/restart capabilities at any stage of the workflow. This is quite important since the propagation portion of the workflow can be very time-consuming and restarts are usually needed in shared computing systems. Moreover, the TAMM RT-EOM-CCSD shows very good scalability, paving the way for simulations of larger, more realistic and chemically relevant systems, employing larger basis sets in conjunction with reduced memory requirements. Illustrative calculations for the formaldehyde and ESCA molecules demonstrate that the predicted positions for the quasiparticle and satellite peaks are in good agreement with experimental values. In particular, the RT-EOM-CCSD reproduced the relative position of the different core ionizations in the ESCA molecule, highlighting its capabilities to study chemical speciation. The method describes the positions of the satellite peaks without any corrections to the quasiparticle-satellite gap.

Finally, work is in progress on an atomic orbital-based implementation, coupled to more efficient solvers for the implicit Adams–Moulton propagator that should reduce the computational time by at least an order of magnitude. Other future methodological developments include the implementation of spin-orbit coupling, and the multi-component coupled-cluster formalism. These extensions will allow first-principles studies of multielectron dynamics in previously unreachable large chemical systems, such as simulations involving multiple core holes.

Acknowledgement This work was supported by the Computational Chemical Sciences Program of

the U.S. Department of Energy, Office of Science, BES, Chemical Sciences, Geosciences and Biosciences Division in the Center for Scalable and Predictive methods for Excitations and Correlated phenomena (SPEC) at PNNL, with computational support from NERSC, a DOE Office of Science User Facility, under contract no. DE-AC02-05CH11231. B.P. also acknowledges support from the Laboratory Directed Research and Development (LDRD) Program at PNNL.

References

- (1) Meirer, F.; Weckhuysen, B. M. Spatial and temporal exploration of heterogeneous catalysts with synchrotron radiation. *Nat. Rev. Mater.* **2018**, *3*, 324–340.
- (2) Qiao, S.; He, Q.; Zhang, P.; Zhou, Y.; Chen, S.; Song, L.; Wei, S. Synchrotron-radiation spectroscopic identification towards diverse local environments of single-atom catalysts. *J. Mater. Chem. A* **2022**, *10*, 5771–5791.
- (3) Kunin, A.; Neumark, D. M. Time-resolved radiation chemistry: femtosecond photoelectron spectroscopy of electron attachment and photodissociation dynamics in iodide–nucleobase clusters. *Phys. Chem. Chem. Phys.* **2019**, *21*, 7239–7255.
- (4) Seah, M. The quantitative analysis of surfaces by XPS: A review. *Surf. Interface Anal.* **1980**, *2*, 222–239.
- (5) Bagus, P. S.; Ilton, E. S.; Nelin, C. J. The interpretation of XPS spectra: Insights into materials properties. *Surf. Sci. Rep.* **2013**, *68*, 273–304.
- (6) Shchukarev, A. XPS at solid–aqueous solution interface. *Adv. Colloid Interface Sci.* **2006**, *122*, 149–157.
- (7) Coester, F. Bound states of a many-particle system. *Nucl. Phys.* **1958**, *7*, 421–424.
- (8) Coester, F.; Kümmel, H. Short-range correlations in nuclear wave functions. *Nucl. Phys.* **1960**, *17*, 477–485.

- (9) Čížek, J. On the Correlation Problem in Atomic and Molecular Systems. Calculation of Wavefunction Components in Ursell-Type Expansion Using Quantum-Field Theoretical Methods. *J. Chem. Phys.* **1966**, *45*, 4256–4266.
- (10) Paldus, J.; Čížek, J.; Shavitt, I. Correlation Problems in Atomic and Molecular Systems. IV. Extended Coupled-Pair Many-Electron Theory and Its Application to the BH₃ Molecule. *Phys. Rev. A* **1972**, *5*, 50–67.
- (11) Kümmel, H. G. A biography of the coupled cluster method. *Int. J. Mod. Phys. B* **2003**, *17*, 5311–5325.
- (12) Bartlett, R. J.; Musiał, M. Coupled-cluster theory in quantum chemistry. *Rev. Mod. Phys.* **2007**, *79*, 291–352.
- (13) Mukherjee, D.; Pal, S. Use of cluster expansion methods in the open-shell correlation problem. *Adv. Quantum Chem.* **1989**, *20*, 291–373.
- (14) Krylov, A. I. Equation-of-motion coupled-cluster methods for open-shell and electronically excited species: the Hitchhiker’s guide to Fock space. *Annu. Rev. Phys. Chem.* **2008**, *59*, 433–462.
- (15) Piecuch, P.; Kowalski, K.; Pimienta, I. S.; Mcguire, M. J. Recent advances in electronic structure theory: Method of moments of coupled-cluster equations and renormalized coupled-cluster approaches. *Int. Rev. Phys. Chem.* **2002**, *21*, 527–655.
- (16) Crawford, T. D.; Schaefer, H. F. An introduction to coupled cluster theory for computational chemists. *Rev. Comput. Chem.* **2000**, *14*, 33–136.
- (17) Nooijen, M.; Snijders, J. G. Coupled cluster approach to the single-particle Green’s function. *Int. J. Quantum Chem.* **1992**, *44*, 55–83.
- (18) Nooijen, M.; Snijders, J. G. Coupled cluster Green’s function method: Working equations and applications. *Int. J. Quantum Chem.* **1993**, *48*, 15–48.
- (19) Nooijen, M.; Snijders, J. G. Second order many-body perturbation approximations to the coupled cluster Green’s function. *J. Chem. Phys.* **1995**, *102*, 1681–1688.
- (20) Meissner, L.; Bartlett, R. J. Electron propagator theory with the ground state correlated by the coupled-cluster method. *Int. J. Quantum Chem.* **1993**, *48*, 67–80.
- (21) Bhaskaran-Nair, K.; Kowalski, K.; Shelton, W. A. Coupled cluster Green function: Model involving single and double excitations. *J. Chem. Phys.* **2016**, *144*, 144101.
- (22) Peng, B.; Kowalski, K. Coupled-cluster Green’s function: Analysis of properties originating in the exponential parametrization of the ground-state wave function. *Phys. Rev. A* **2016**, *94*, 062512.
- (23) Peng, B.; Kowalski, K. Properties of advanced coupled-cluster Green’s function. *Mol. Phys.* **2018**, *116*, 561–569.
- (24) Peng, B.; Bauman, N. P.; Gulania, S.; Kowalski, K. *Annu. Rep. Comput. Chem.*; Elsevier, 2021; Vol. 17; pp 23–53.
- (25) Shee, A.; Zgid, D. Coupled Cluster as an impurity solver for Green’s function embedding methods. *J. Chem. Theory Comput.* **2019**, *15*, 6010–6024.
- (26) Lange, M. F.; Berkelbach, T. C. On the relation between equation-of-motion coupled-cluster theory and the GW approximation. *J. Chem. Theory Comput.* **2018**, *14*, 4224–4236.
- (27) Hoodbhoy, P.; Negele, J. Time-dependent coupled-cluster approximation to nuclear dynamics. I. Application to a solvable model. *Phys. Rev. C* **1978**, *18*, 2380.
- (28) Hoodbhoy, P.; Negele, J. Time-dependent coupled-cluster approximation to nuclear dynamics. II. General formulation. *Phys. Rev. C* **1979**, *19*, 1971.
- (29) Schönhammer, K.; Gunnarsson, O. Time-dependent approach to the calculation of

- spectral functions. *Phys. Rev. B* **1978**, *18*, 6606.
- (30) Kvaal, S. Ab initio quantum dynamics using coupled-cluster. *J. Chem. Phys.* **2012**, *136*, 194109.
- (31) Arponen, J. Variational principles and linked-cluster exp S expansions for static and dynamic many-body problems. *Ann. Phys.* **1983**, *151*, 311–382.
- (32) Sato, T.; Pathak, H.; Orimo, Y.; Ishikawa, K. L. Communication: Time-dependent optimized coupled-cluster method for multielectron dynamics. *J. Chem. Phys.* **2018**, *148*, 051101.
- (33) Pathak, H.; Sato, T.; Ishikawa, K. L. Time-dependent optimized coupled-cluster method for multielectron dynamics. II. A coupled electron-pair approximation. *J. Chem. Phys.* **2020**, *152*, 124115.
- (34) Caillat, J.; Zanghellini, J.; Kitzler, M.; Koch, O.; Kreuzer, W.; Scrinzi, A. Correlated multielectron systems in strong laser fields: A multiconfiguration time-dependent Hartree-Fock approach. *Phys. Rev. A* **2005**, *71*, 012712.
- (35) Kato, T.; Kono, H. Time-dependent multi-configuration theory for electronic dynamics of molecules in an intense laser field. *Chem. Phys. Lett.* **2004**, *392*, 533–540.
- (36) Sato, T.; Ishikawa, K. L. Time-dependent complete-active-space self-consistent-field method for multielectron dynamics in intense laser fields. *Phys. Rev. A* **2013**, *88*, 023402.
- (37) Ishikawa, K. L.; Sato, T. A review on ab initio approaches for multielectron dynamics. *IEEE J. Sel. Top. Quantum Electron* **2015**, *21*, 1–16.
- (38) Sato, T.; Pathak, H.; Orimo, Y.; Ishikawa, K. L. Time-dependent multi-configuration self-consistent-field and time-dependent optimized coupled-cluster methods for intense laser-driven multielectron dynamics. *arXiv preprint arXiv:2211.10116* **2022**,
- (39) Pathak, H.; Sato, T.; Ishikawa, K. L. Time-dependent optimized coupled-cluster method for multielectron dynamics. III. A second-order many-body perturbation approximation. *J. Chem. Phys.* **2020**, *153*, 034110.
- (40) Pathak, H.; Sato, T.; Ishikawa, K. L. Study of laser-driven multielectron dynamics of Ne atom using time-dependent optimised second-order many-body perturbation theory. *Mol. Phys.* **2020**, *118*, e1813910.
- (41) Li, X.; Govind, N.; Isborn, C.; De-Prince III, A. E.; Lopata, K. Real-time time-dependent electronic structure theory. *Chem. Rev.* **2020**, *120*, 9951–9993.
- (42) Monkhorst, H. J. Calculation of Properties with the Coupled-Cluster Method. *Int. J. Quantum Chem.* **1977**, *12*, 421–432.
- (43) Mukherjee, D.; Mukherjee, P. A response-function approach to the direct calculation of the transition-energy in a multiple-cluster expansion formalism. *Chem. Phys.* **1979**, *39*, 325–335.
- (44) Guha, S.; Mukherjee, D. A multireference coupled-cluster approach to quantum dynamics. *Chem. Phys. Lett.* **1991**, *186*, 84–90.
- (45) Dalgaard, E.; Monkhorst, H. J. Some aspects of the time-dependent coupled-cluster approach to dynamic response functions. *Phys. Rev. A* **1983**, *28*, 1217.
- (46) Koch, H.; Jørgensen, P. Coupled cluster response functions. *J. Chem. Phys.* **1990**, *93*, 3333–3344.
- (47) Takahashi, M.; Paldus, J. Time-dependent coupled cluster approach: Excitation energy calculation using an orthogonally spin-adapted formalism. *J. Chem. Phys.* **1986**, *85*, 1486–1501.
- (48) Prasad, M. D. Time-dependent coupled cluster method: A new approach to the calculation of molecular absorption spectra. *J. Chem. Phys.* **1988**, *88*, 7005–7010.

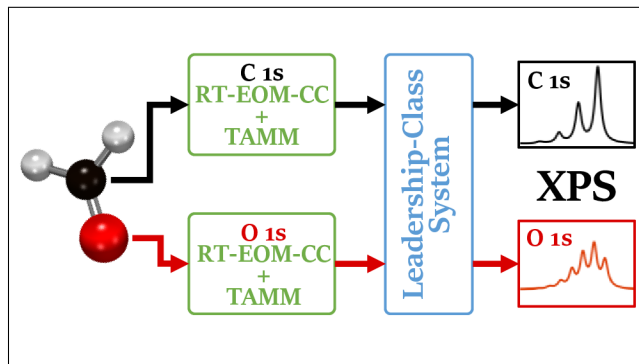
- (49) Sebastian, K. Correlation effects in ion neutralization scattering with the use of a time-dependent coupled-cluster approach. *Phys. Rev. B* **1985**, *31*, 6976.
- (50) Pigg, D. A.; Hagen, G.; Nam, H.; Papenbrock, T. Time-dependent coupled-cluster method for atomic nuclei. *Phys. Rev. C* **2012**, *86*, 014308.
- (51) Nascimento, D. R.; DePrince III, A. E. Linear absorption spectra from explicitly time-dependent equation-of-motion coupled-cluster theory. *J. Chem. Theory Comput.* **2016**, *12*, 5834–5840.
- (52) Nascimento, D. R.; DePrince III, A. E. Simulation of near-edge X-ray absorption fine structure with time-dependent equation-of-motion coupled-cluster theory. *J. Phys. Chem. Lett.* **2017**, *8*, 2951–2957.
- (53) Koulias, L. N.; Williams-Young, D. B.; Nascimento, D. R.; DePrince III, A. E.; Li, X. Relativistic real-time time-dependent equation-of-motion coupled-cluster. *J. Chem. Theory Comput.* **2019**, *15*, 6617–6624.
- (54) Nascimento, D. R.; DePrince III, A. E. A general time-domain formulation of equation-of-motion coupled-cluster theory for linear spectroscopy. *J. Chem. Phys.* **2019**, *151*, 204107.
- (55) Pathak, H.; Sato, T.; Ishikawa, K. L. Time-dependent optimized coupled-cluster method for multielectron dynamics. IV. Approximate consideration of the triple excitation amplitudes. *J. Chem. Phys.* **2021**, *154*, 234104.
- (56) Park, Y. C.; Perera, A.; Bartlett, R. J. Equation of motion coupled-cluster for core excitation spectra: Two complementary approaches. *J. Chem. Phys.* **2019**, *151*, 164117.
- (57) Huber, C.; Klamroth, T. Explicitly time-dependent coupled cluster singles doubles calculations of laser-driven many-electron dynamics. *J. Chem. Phys.* **2011**, *134*, 054113.
- (58) Shushkov, P.; Miller III, T. F. Real-time density-matrix coupled-cluster approach for closed and open systems at finite temperature. *J. Chem. Phys.* **2019**, *151*, 134107.
- (59) White, A. F.; Chan, G. K.-L. A Time-Dependent Formulation of Coupled-Cluster Theory for Many-Fermion Systems at Finite Temperature. *J. Chem. Theory Comput.* **2018**, *14*, 5690–5700.
- (60) Pedersen, T. B.; Kvaal, S. Symplectic integration and physical interpretation of time-dependent coupled-cluster theory. *J. Chem. Phys.* **2019**, *150*, 144106.
- (61) Rehr, J. J.; Vila, F. D.; Kas, J. J.; Hirshberg, N. Y.; Kowalski, K.; Peng, B. Equation of motion coupled-cluster cumulant approach for intrinsic losses in x-ray spectra. *J. Chem. Phys.* **2020**, *152*, 174113.
- (62) Vila, F. D.; Rehr, J. J.; Kas, J. J.; Kowalski, K.; Peng, B. Real-time coupled-cluster approach for the cumulant Green’s function. *J. Chem. Theory Comput.* **2020**, *16*, 6983–6992.
- (63) Vila, F. D.; Kas, J. J.; Rehr, J. J.; Kowalski, K.; Peng, B. Equation-of-Motion Coupled-Cluster Cumulant Green’s Function for Excited States and X-Ray Spectra. *Front. Chem.* **2021**, *9*, 734945.
- (64) Vila, F.; Kowalski, K.; Peng, B.; Kas, J.; Rehr, J. Real-Time Equation-of-Motion CCSD Cumulant Green’s Function. *J. Chem. Theory Comput.* **2022**, *18*, 1799–1807.
- (65) Vila, F.; Rehr, J.; Pathak, H.; Peng, B.; Panyala, A.; Mutlu, E.; Bauman, N.; Kowalski, K. Real-time equation-of-motion CC cumulant and CC Green’s function simulations of photoemission spectra of water and water dimer. *J. Chem. Phys.* **2022**, *157*, 044101.
- (66) Mutlu, E.; Panyala, A.; Kowalski, K.; Bauman, N.; Peng, B.; Brabec, J.; Krishnamoorthy, S. TAMM: Tensor Algebra for Many-body Methods. *arXiv preprint arXiv:2201.01257* **2022**,

- (67) Mutlu, E.; Kowalski, K.; Krishnamoorthy, S. Toward generalized tensor algebra for ab initio quantum chemistry methods. Proceedings of the 6th ACM SIGPLAN International Workshop on Libraries, Languages and Compilers for Array Programming. 2019; pp 46–56.
- (68) Peng, B.; Kowalski, K. Low-rank factorization of electron integral tensors and its application in electronic structure theory. *Chem. Phys. Lett.* **2017**, *672*, 47–53.
- (69) Peng, B.; Kowalski, K. Highly efficient and scalable compound decomposition of two-electron integral tensor and its application in coupled cluster calculations. *J. Chem. Theory Comput.* **2017**, *13*, 4179–4192.
- (70) Kas, J. J.; Rehr, J. J.; Reining, L. Cumulant expansion of the retarded one-electron Green function. *Phys. Rev. B* **2014**, *90*, 085112.
- (71) Kas, J. J.; Vila, F. D.; Rehr, J. J.; Chambers, S. A. Real-time cumulant approach for charge-transfer satellites in x-ray photoemission spectra. *Phys. Rev. B* **2015**, *91*, 121112.
- (72) Kas, J. J.; Rehr, J. J.; Curtis, J. B. Particle-hole cumulant approach for inelastic losses in x-ray spectra. *Phys. Rev. B* **2016**, *94*, 035156.
- (73) Rehr, J. J.; Kas, J. J. Strengths of plasmon satellites in XPS: Real-time cumulant approach. *J. Vac. Sci. Technol. A* **2021**, *39*, 060401.
- (74) Quarteroni, A.; Sacco, R.; Saleri, F. *Numerical mathematics*; Springer Science & Business Media, 2010; Vol. 37.
- (75) Nieplocha, J.; Palmer, B.; Tipparaju, V.; Krishnan, M.; Trease, H.; Aprà, E. Advances, Applications and Performance of the Global Arrays Shared Memory Programming Toolkit. *The International Journal of High Performance Computing Applications* **2006**, *20*, 203–231.
- (76) Van Zee, F. G.; van de Geijn, R. A. BLIS: A Framework for Rapidly Instantiating BLAS Functionality. *ACM Transactions on Mathematical Software* **2015**, *41*, 14:1–14:33.
- (77) Springer, P.; Su, T.; Bientinesi, P. HPTT: A High-Performance Tensor Transposition C++ Library. **2017**, 56–62.
- (78) Lyakh, D. I. TAL-SH: Tensor Algebra Library for Shared Memory Computers: Nodes equipped with multicore CPU, Nvidia GPU, and Intel Xeon Phi. https://github.com/DmitryLyakh/TAL_SH, 2019.
- (79) Valeev, E. F. Libint - a library for the evaluation of molecular integrals of many-body operators over Gaussian functions. <https://github.com/evaleev/libint>, 2019.
- (80) Kowalski, K.; Bair, R.; Bauman, N. P.; Boschen, J. S.; Bylaska, E. J.; Daily, J.; de Jong, W. A.; Dunning Jr, T.; Govind, N.; Harrison, R. J., et al. From NWChem to NWChemEx: Evolving with the computational chemistry landscape. *Chem. Rev.* **2021**, *121*, 4962–4998.
- (81) Gunnels, J. A.; Gustavson, F. G.; Henry, G. M.; Van De Geijn, R. A. FLAME: Formal linear algebra methods environment. *ACM Trans. Math. Softw.* **2001**, *27*, 422–455.
- (82) Solomonik, E.; Matthews, D.; Hammond, J. R.; Stanton, J. F.; Demmel, J. A massively parallel tensor contraction framework for coupled-cluster computations. *J. Parallel Distrib. Comput.* **2014**, *74*, 3176–3190.
- (83) Epifanovsky, E.; Wormit, M.; Kuś, T.; Landau, A.; Zuev, D.; Khistyayev, K.; Manohar, P.; Kaliman, I.; Dreuw, A.; Krylov, A. I. New implementation of high-level correlated methods using a general block tensor library for high-performance electronic structure calculations. *Wiley Online Library* **2013**,
- (84) Ibrahim, K. Z.; Williams, S. W.; Epifanovsky, E.; Krylov, A. I. Analysis and tuning of libtensor framework on multicore

architectures. 2014 21st International Conference on High Performance Computing (HiPC). 2014; pp 1–10.

- (85) Røeggen, I.; Wisløff-Nilssen, E. On the Beebe-Linderberg two-electron integral approximation. *Chem. Phys. Lett.* **1986**, *132*, 154–160.
- (86) Koch, H.; Sánchez de Merás, A.; Pedersen, T. B. Reduced scaling in electronic structure calculations using Cholesky decompositions. *J. Chem. Phys.* **2003**, *118*, 9481–9484.
- (87) Beebe, N. H.; Linderberg, J. Simplifications in the generation and transformation of two-electron integrals in molecular calculations. *Int. J. Quantum Chem.* **1977**, *12*, 683–705.
- (88) Aquilante, F.; Pedersen, T. B.; Lindh, R. Low-cost evaluation of the exchange Fock matrix from Cholesky and density fitting representations of the electron repulsion integrals. *J. Chem. Phys.* **2007**, *126*, 194106.
- (89) Røeggen, I.; Johansen, T. Cholesky decomposition of the two-electron integral matrix in electronic structure calculations. *J. Chem. Phys.* **2008**, *128*, 194107.
- (90) <https://cccbdb.nist.gov/>.
- (91) Kendall, R. A.; Dunning Jr, T. H.; Harrison, R. J. Electron affinities of the first-row atoms revisited. Systematic basis sets and wave functions. *J. Chem. Phys.* **1992**, *96*, 6796–6806.
- (92) Noro, T.; Sekiya, M.; Koga, T. Contracted polarization functions for the atoms helium through neon. *Theor. Chem. Acc.* **1997**, *98*, 25–32.
- (93) Noro, T.; Sekiya, M.; Koga, T. Correlating basis sets for the H atom and the alkali-metal atoms from Li to Rb. *Theor. Chem. Acc.* **2003**, *109*, 85–90.
- (94) Travnikova, O.; Patanen, M.; Soderstrom, J.; Lindblad, A.; Kas, J. J.; Vila, F. D.; Céolin, D.; Marchenko, T.; Goldsztejn, G.; Guillemin, R., et al. Energy-Dependent Relative Cross Sections in Carbon 1s Photoionization: Separation of Direct Shake and Inelastic Scattering Effects in Single Molecules. *J. Phys. Chem. A* **2019**, *123*, 7619–7636.
- (95) Kuramoto, K.; Ehara, M.; Nakatsuji, H.; Kitajima, M.; Tanaka, H.; De Fanis, A.; Tamenori, Y.; Ueda, K. C 1s and O 1s photoelectron spectra of formaldehyde with satellites: theory and experiment. *J. Electron. Spectros. Relat. Phenomena* **2005**, *142*, 253–259.

Graphical TOC Entry



For Table of Contents Only